Atmospheric Environment 209 (2019) 67–77

Contents lists available at ScienceDirect

Atmospheric Environment

journal homepage: www.elsevier.com/locate/atmosenv

Impact of dust-polluted convective clouds over the Tibetan Plateau on downstream precipitation

Yuzhi Liu, Qingzhe Zhu, Jianping Huang*, Shan Hua, Rui Jia

Key Laboratory for Semi-Arid Climate Change of the Ministry of Education, College of Atmospheric Sciences, Lanzhou University, Lanzhou, 730000, China

ARTICLE INFO

Keywords:
Aerosols
Tibetan plateau
Convective clouds
Precipitation

ABSTRACT

Based on satellite observations and reanalysis datasets, this study focuses on the effect of aerosols on clouds over the Tibetan Plateau (TP) and the impact of dust-polluted convective clouds on precipitation over downstream regions. A heavy dust event is detected by Cloud-Aerosol Lidar and Infrared Pathfinder Satellite Observations (CALIPSO) over the northern slope of the TP on 16 July and 17 July 2016. The high aerosol optical depth (AOD) values are mainly distributed over the northern slope of the TP. Simultaneously, the CloudSat satellite observes deep convective clouds over the northern slope area of the TP, in which convective clouds and dust mix at the same height. With the AOD increasing from 16 July to its peak on 17 July, the ice particle size decreases to a minimum, and convective clouds develop at higher heights because of the prolonged cloud life. Accordingly, a larger ice water path (IWP) is induced by the development of convective clouds that move eastwardly from 16 to 17 July. In the following days, under favorable meteorological conditions, some of the developed convective clouds continuously move eastward and merge with the convective cloud clusters along the motion path, which induces significant precipitation over the Yangtze River basin on 17 July. Furthermore, driven by the northward wind, some developed convective cloud clusters move northward and induce strong precipitation over North China on 19 July. The indirect effect of dust aerosols over the TP could enhance the plateau's cloud development and potentially contribute to downstream precipitation, which is a meaningful factor for weather forecasting.

1. Introduction

With the increase in human activities, aerosols are becoming one of the most important factors affecting the climate and environment at regional and global scales (Huang et al., 2014; Liu et al., 2015; Qin et al., 2001; Wang et al., 2015; Zhang, 2010). Aerosol particles affect the Earth's climate system through direct (Huang et al., 2014; Liu et al., 2013, 2014; Sokolik and Toon, 1996; Shi et al., 2005), indirect and semidirect (Huang et al., 2006a; Huang et al., 2010; Sassen, 2002) radiative effects. Currently, the impacts of aerosols on clouds and precipitation are still uncertain. Huang et al. (2006b) and Wang et al. (2010) found that aerosols driven into clouds can reduce the ice-cloud effective particle size and optical depth of cirrus clouds over northwestern China. Moreover, Rosenfeld and Woodley (2000) suggested that aerosols can hinder warm shallow clouds and promote deep convective clouds. Koch and Del Genio (2010) found a similar phenomenon in which aerosols below the cloud layer can increase the coverage of convective clouds. In addition, previous studies have shown that aerosol-cloud interactions have a suppressive effect on light rain (Andreae et al., 2004; Huang et al., 2009; Khain et al., 2008; Qian et al., 2009) and a stimulative effect on heavy rain (Petters et al., 2006; Rosenfeld et al., 2008; Tao et al., 2012).

The Tibetan Plateau (TP) is the highest-elevated landmark in the world, with elevations ranging from approximately 1500 to 5000 m above sea level. The TP plays a significant role in adjusting atmospheric circulation and climate change over the Northern Hemisphere, especially over Asia (Duan and Wu, 2005; Manabe et al., 1974; Shi et al., 2015; Tang et al., 2013; Wu et al., 2007; Zhou et al., 2009; Hua et al., 2018). Zhang et al. (2001) reported that dust aerosols are the major type of aerosols over the TP. Based on satellite observations and a trajectory model, Jia et al. (2015) found that dust aerosols over the TP are mainly transported from the Taklimakan Desert in summer. The addition of aerosols to the atmosphere is a new threat for the TP.

The aerosols transported to the TP may affect the hydrological and monsoon cycles in India and East Asia (Huang et al., 2009; Kuhlmann and Quaas, 2010; Lau et al., 2010). In addition, the TP is a relatively active area for convective clouds and mesoscale convective systems due to its elevated heating effect in the summer. The eastward movement of convective clouds away from the TP could cause heavy rainfall over the middle and lower reaches of the Yangtze River (Liu et al., 2007).

* Corresponding author
E-mail address: hjp@lzu.edu.cn (J. Huang).

https://doi.org/10.1016/j.atmosenv.2019.04.001
Received 21 February 2019; Received in revised form 29 March 2019; Accepted 2 April 2019
Available online 06 April 2019

Although many studies have addressed aerosols over the plateau, the effect of aerosols on convective clouds and the additional impact of polluted clouds on downstream precipitation are unclear.

In this study, a heavy dust event and dust-convective cloud mixtures over the TP on 16–17 July 2016 are considered. By combining several datasets (i.e., the Cloud-Aerosol Lidar and Infrared Pathfinder Satellite Observations (CALIPSO), CloudSat, Clouds and the Earth's Radiant Energy System (CERES), Moderate Resolution Imaging Spectroradiometer (MODIS), Tropical Rainfall Measuring Mission (TRMM), the Fengyun (FY)-2E satellite and the second Modern-Era Retrospective analysis for Research and Applications (MERRA-2) datasets, the effect of aerosols on convective clouds over the TP and the impact of polluted convective clouds moving away from the TP towards downstream regions are investigated.

2. Datasets

2.1. CALIPSO profiles

The Cloud-Aerosol Lidar with Orthogonal Polarization (CALIOP) sensor carried on the CALIPSO satellite is a two-wavelength, polarization-sensitive backscatter lidar that exhibits strong sensitivity in the detection of aerosols and clouds and can therefore acquire their vertical information (Winker and Pelon, 2004; Liu et al., 2009). In this study, data consisting of the total and perpendicular attenuated backscatter coefficients at 532 nm from the CALIPSO Version 4 Level 1B product and data comprising aerosol particle properties such as classified particles from the Version 4 Level 2 CALIPSO lidar Vertical Feature Mask (VFM) product are used to identify dust events. These products are archived and contributed by the Atmospheric Science Data Center (ASDC).

2.2. CERES profiles

CERES is one of the highest-priority scientific satellite instruments developed for the Earth Observing System (EOS) and provides the first long-term global estimates of the radiative fluxes in Earth's atmosphere. In this study, the 1-hourly SYN1deg_Ed4A product, with a resolution of $1^\circ \times 1^\circ$, is used to analyze cloud properties including ice water path, cloud area fraction and cloud top height. The CERES data are obtained from the ASDC at the NASA Langley Research Center (Chambers et al., 2002).

2.3. CloudSat profiles

CloudSat is the first satellite equipped with a 94 GHz Cloud Profiling Radar (CPR), with an orbital resolution of 2.5 km, horizontal resolution of 1.4 km, and a total of 125 vertical layers in the vertical direction, each with a thickness of 240 m. The cloud classification product (2B_CLDCLASS) of CloudSat is a combination of CPR, CALIPSO, and MODIS data and distinguishes classifications based on different cloud, structure, and physical characteristics. The specific classification classifies clouds into 8 categories: Altocumulus (Ac), Altostratus (As), Cumulus (Cu), Deep Convective Cloud (Dc), Nimbostratus (Ns), Stratus (St), Stratocumulus (Sc), and Cirrus (Ci). In this study, the 2B-CLDCLASS_GRANULE product is used to identify cloud categories over the TP. The CloudSat data are obtained from the Cooperative Institute for Research in the Atmosphere at Colorado State University (Stephens et al., 2008; Vane and Stephens, 2008).

2.4. MODIS profiles

MODIS is an optical remote sensor onboard the Terra and Aqua satellites that provides global observations at wavelengths ranging from the visible band to the mid-infrared band. In this study, the MOD08_D3 product, with a resolution of $1^\circ \times 1^\circ$, is used to analyze the variation in cloud aerosol properties. MODIS product archived at the Atmosphere Archive and Distribution System (LAADS) Distributed Active Archive Center (DAAC) (Ackerman et al., 1998; Engel-Cox et al., 2004).

2.5. TRMM profiles

The TRMM pilot project is a tropical precipitation measurement project that was jointly conducted by NASA (National Aeronautics and Space Administration) and NASDA (National Space Development Agency). The TRMM satellite can provide precipitation data for the region from 50°N to 50°S. In this study, the TRMM 3-hourly 3B42 v7 product, with a resolution of $0.5^\circ \times 0.5^\circ$, is used to display the spatial and temporal distributions of precipitation over China. The TRMM data are obtained from the NASA's Goddard Space Flight Center (Simpson et al., 1998; Lonfat, 2004).

2.6. FY-2E profiles

The FY-2 meteorological satellite is a first-generation geostationary meteorological satellite developed in China. FY-2E is the third Fengyun series of stationary satellites, which was launched on 23 December 2008 (Zou et al., 2011; Wang and Li, 2014). In this study, hourly black body temperature (TBB) data, with a resolution of 5 km, from the FY-2E profiles were used to study the movement of convective clouds. The FY-2E data are provided by the National Satellite Meteorological Center of the Chinese Meteorology Administration (http://www.nsmc.cma.gov.cn/).

2.7. MERRA-2 data

MERRA-2 is a long-term atmospheric reanalysis dataset, and it starts in 1980. MERRA-2 is also the first satellite-era global reanalysis to assimilate the space-based observations of aerosols and represent their interactions with other physical processes in the climate system. All data collections from MERRA-2 are at the regular longitude-by-latitude grid of $0.625^\circ \times 0.5^\circ$ (Molod et al., 2015; Gelaro et al., 2017). In this study, the hourly aerosol diagnostics product of tavg1_2d_aer_Nx from MERRA-2 is used, and the hourly meteorological contours of the U and V components of the wind speed and geopotential height are used to analyze meteorological conditions. The MERRA-2 data are provided by the NASA Global Modeling and Assimilation Office (https://disc.gsfc.nasa.gov/daac-bin/FTPSubset2.pl/).

2.8. ECMWF data

The Copernicus Climate Change Service (C3S) operated by the European Center for Medium-Range Weather Forecasts (ECMWF) released a new global climate monitoring dataset, ERA5, on 17 July 2017 (Hersbach, 2016). In this study, the hourly ERA5 reanalysis data are used to analyze the variation in relative humidity. The reanalysis data have a spatial (latitudinal and longitudinal) resolution of $0.25^\circ \times 0.25^\circ$.

3. Analysis results

The TP extends over a region of 25–40°N, 74–104°E, as shown by the area enclosed within the purple line in Fig. 1. The TP is located at the juncture of several important natural and anthropogenic aerosol sources. The Taklimakan Desert lies to the north, the Gobi Desert lies to the northeast, and the Great Indian Desert lies to the southwest. To discuss the influence of the TP on precipitation over downstream regions, North China (red rectangle in Fig. 1) and the Yangtze River basin (blue rectangle in Fig. 1) are the downstream regions of concern in this study.

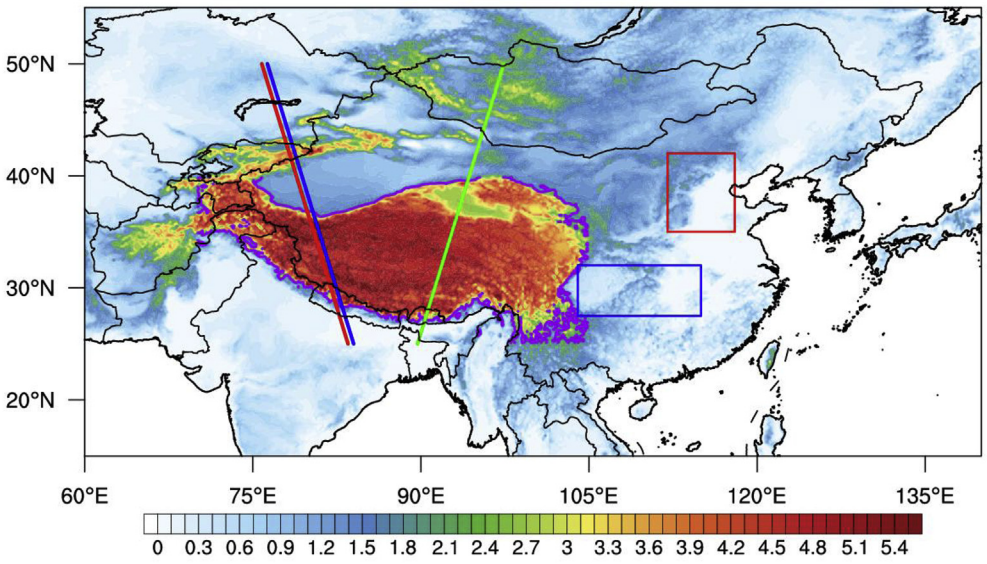

Fig. 1. Topography in the vicinity of the TP; the contours of terrain height are in km (above mean sea level). The thick purple solid curve indicates the main area of the TP. The solid red and green lines indicate the trajectories of the CALIPSO satellite over the TP on 16 July and 17 July and the solid blue line indicates the trajectories of the CloudSat satellite on 17 July 2016 (as shown in Fig. 3), respectively. The blue and red rectangles indicate the Yangtze River basin and North China, respectively. (For interpretation of the references to color in this figure legend, the reader is referred to the Web version of this article.)

3.1. Detection of aerosols and clouds over the TP

In this section, the CALIPSO and CloudSat products are combined to identify the aerosol and cloud categories, respectively. Fig. 2 shows the altitude-orbit cross-section of the total attenuated backscattering intensity (a1-a2), the depolarization ratio (b1-b2) and the spatial distributions of the cloud and aerosol types (c1-c2) on 16–17 July 2016. The satellite orbit paths of CALIPSO on 16 July, 17 July 2016 are presented by the red and green lines in Fig. 1, respectively. In Fig. 2a1-a2, the gray shading indicates the topography, the white areas denote clouds, the deep blue area denotes the region without signal because of cloud blocking, and the green-yellow-orange color represents aerosols. Omar et al. (2009) reported that the total attenuated backscatter coefficient of aerosols at 532 nm is concentrated within the range from 0.003 to 0.009 $km^{-1}sr^{-1}$, whereas the depolarization ratio of dust aerosols is generally greater than 0.2 and can reach over 0.4 in severe sandstorms (Chiang et al., 2007; Huang et al., 2007a; Xie et al., 2008); these results are shown in Fig. 2b1 and b2 with yellow, orange and red colors. As shown in Fig. 2a1 and b1, the total attenuated backscatter coefficient ranges from 0.002 to 0.008 $km^{-1}sr^{-1}$, and the volume depolarization ratio ranges from 0.2 to 0.4. In particular, over the Taklimakan Desert (region of 36°N-42°N in Fig. 2a1), the total attenuated backscatter values are relatively large, which indicates that the aerosol concentration over this area is quite high. When combined with Fig. 2c1, dust aerosols can be observed over the Taklimakan Desert. Therefore, a strong dust event is observed over the Taklimakan Desert on 16 July 2016; at the same time, dust aerosols lifted towards the northern slope of the TP. As shown in Fig. 2a2, b2 and c2, a small amount of dust aerosols is observed over the northern margin of the TP on 17 July 2016 (the region of 25°N-40°N in Fig. 2a2), which indicates that dust aerosols are transported from the Taklimakan Desert to the TP.

Fig. 3 shows the altitude-orbit cross-section of the total attenuated backscattering intensity, cloud classifications and the spatial distributions of aerosol types over the TP on 17 July 2016. In Fig. 3b, different colors represent different cloud types. The observation times of the

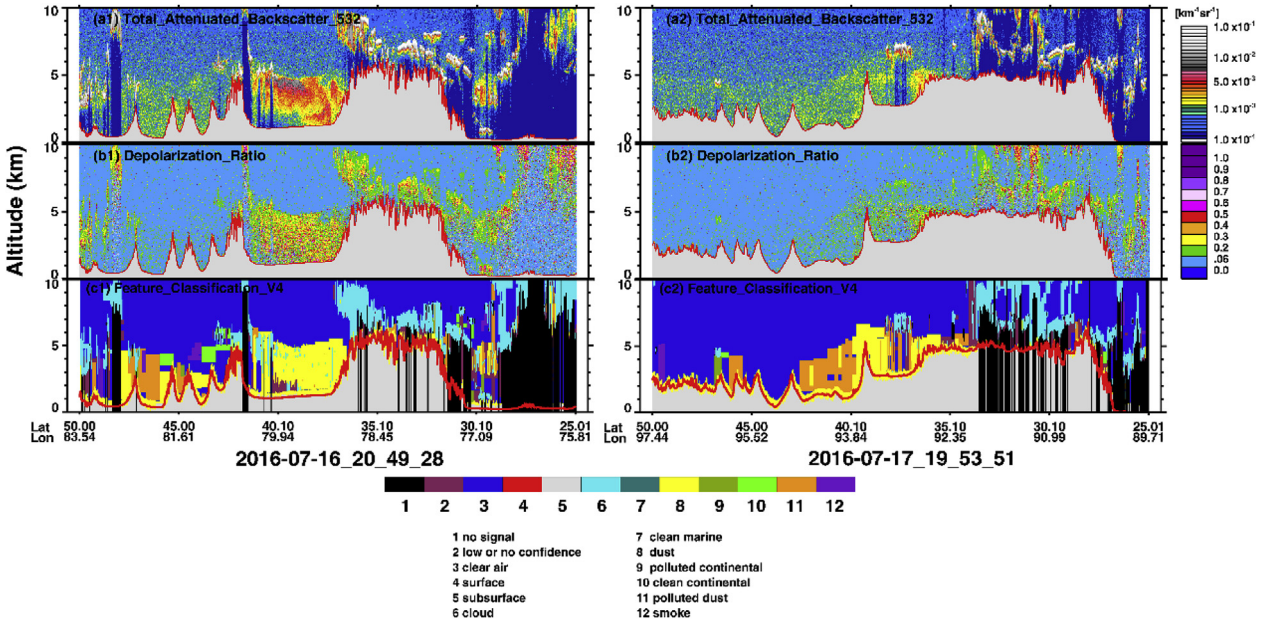

Fig. 2. Altitude-orbit cross-sections of total attenuated backscattering (a1-a2), the depolarization ratio (b1-b2) and classified particles (c1-c2) on 16 July (left column) and 17 July (right column) 2016 along the trajectory of the CALIPSO satellite over the TP.

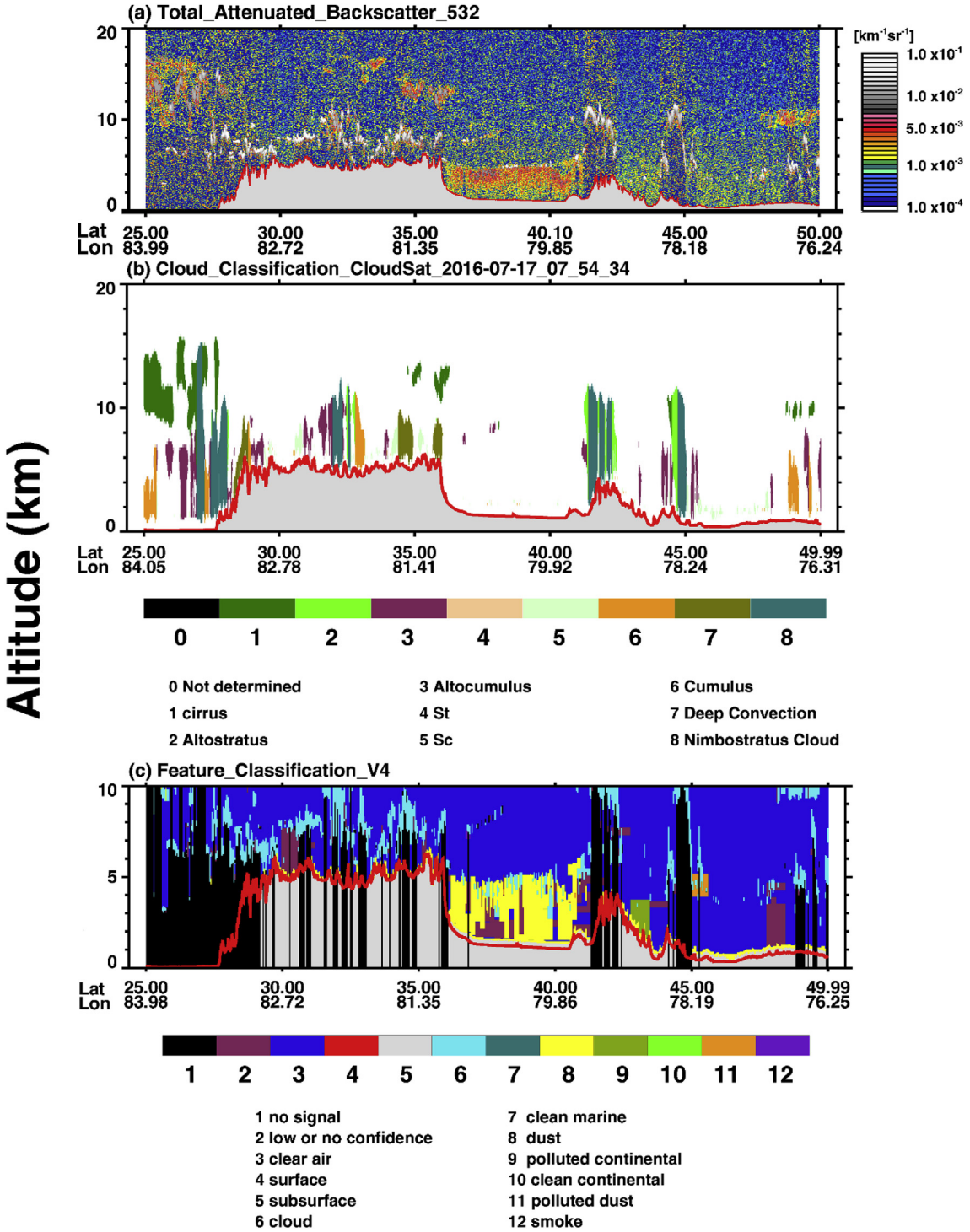

Fig. 3. Altitude-orbit cross-sections of total attenuated backscattering (a), cloud categories (b) and classified particles (c) on 17 July 2016 along the trajectories of the CALIPSO and CloudSat satellites over the TP.

CALIPSO and CloudSat satellites are only 12.5 s apart; therefore, the same area can be observed by these two satellites during nearly the same time period. The orbit paths of these two satellites are represented by the blue line in Fig. 1. As shown in Fig. 3b, there are many kinds of clouds over the TP. The northern margin of the TP is dominated by deep convective clouds, which are accompanied by cirrus clouds. At the bottoms of the deep convective clouds, an upper layer of dust aerosols appears. According to the results of Wang et al. (2010), a mixture of dust aerosols and clouds is considered to occur when dust aerosols are observed to be within 50 m of clouds. Therefore, during the dust event on 17 July 2016, dust aerosols mix with deep convective clouds over the northern slope of the TP.

3.2. Effects of aerosols on convective clouds over the TP

Recent advances have revealed a much more complex interaction of aerosols with clouds (Rosenfeld et al., 2014). Smaller cloud droplets, which are polluted by aerosols, when there is a constant cloud water path, evaporate faster and cause more mixing of ambient air into the cloud top, which could further enhance the evaporation of cloud

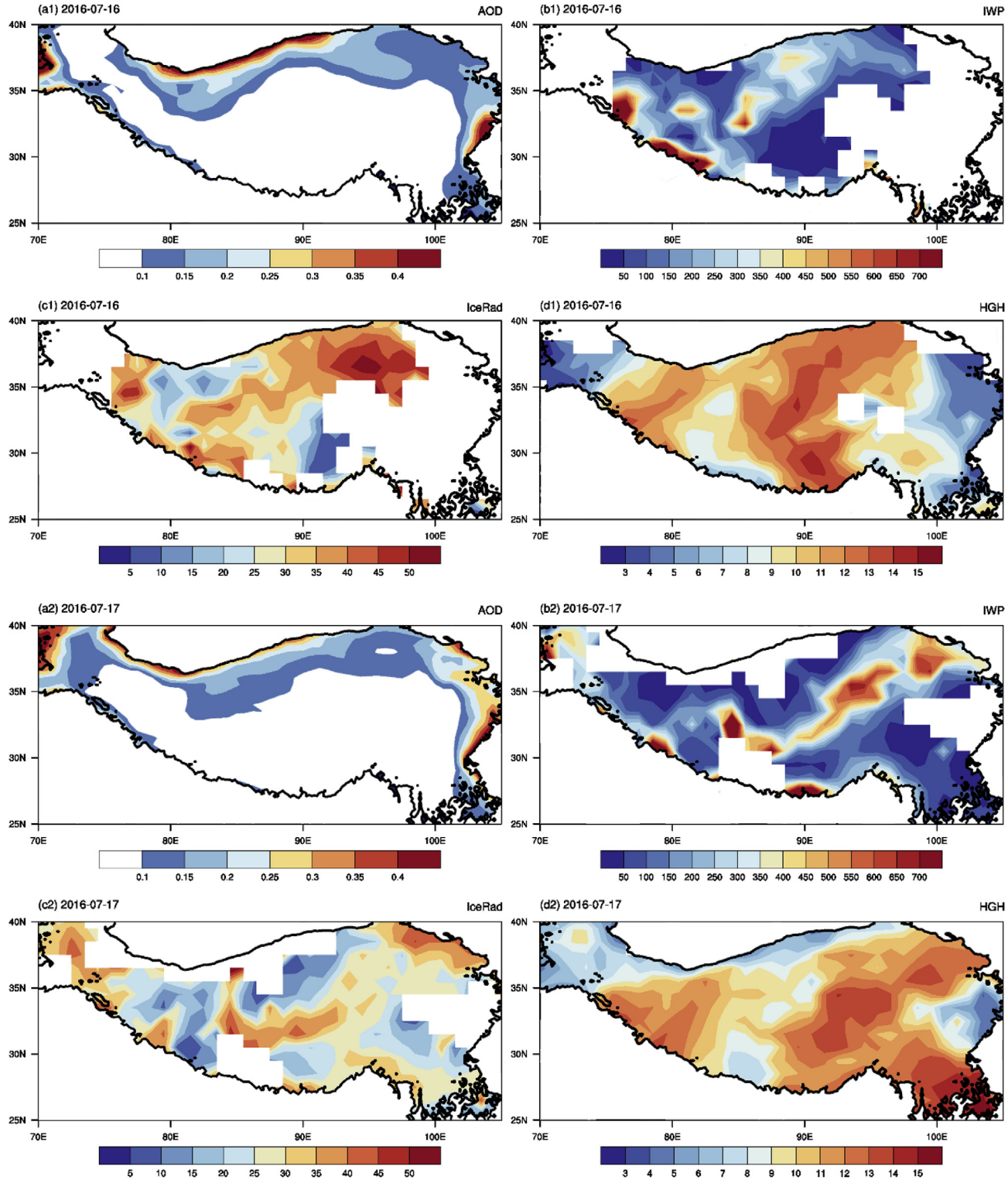

Fig. 4. Distributions of the daily mean AOD (a1 and a2), IWP (b1 and b2; units: g m^2), ice cloud particle radius (c1 and c2; units: μm) and cloud top height (d1 and d2; units: km) over the TP on 16–17 July 2016.

droplets. These small cloud droplets polluted by aerosols could induce an increase in cloud albedo, causing a huge cooling effect through the suppression of precipitation and by extending the cloud lifetime. Additionally, the aerosols may transport large quantities of small ice particles to the anvils of deep convective clouds, leading to a warming effect through the reduction of thermal radiation emitted to space. Though the contributions of individual processes to the overall aerosol-cloud interaction cannot be easily separated, overall, aerosol-cloud interaction includes the indirect radiative effect (consists two components: the albedo effect and the lifetime effect) and semi-direct radiative effect. The previous studies suggested that almost all indirect radiative effect values are negative (Menon et al., 2002; Lohmann and Feichter, 2001; Liu et al., 2014). On the contrary, positive values of semi-direct radiative effect were found in many studies (Cook and

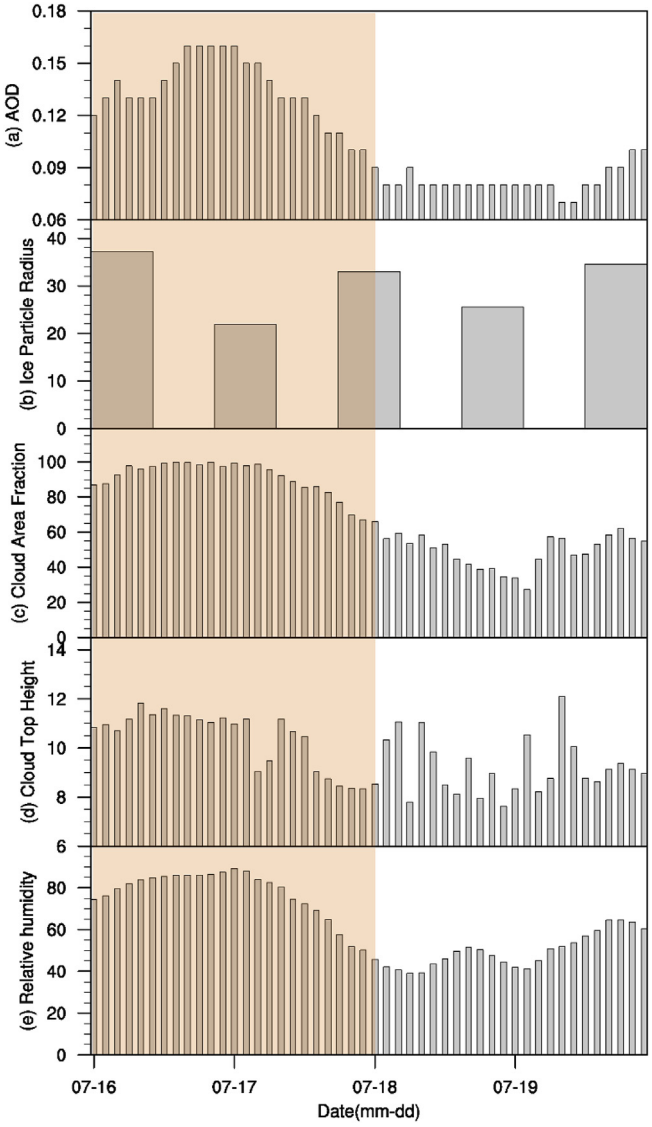

Fig. 5. Time series of the hourly mean (a) AOD from MERRA; cloud properties, including (b) daily mean ice particle radius (units: μm), from MODIS; (c) hourly mean cloud area fraction (units: percent) and (d) cloud top height (units: km) from CERES; and (e) hourly mean relative humidity (units: percent) from ERA5. The yellow shaded area indicates the duration from 16 to 17 July 2016. (For interpretation of the references to color in this figure legend, the reader is referred to the Web version of this article.)

Highwood, 2004; Hansen et al., 1997; Huang et al., 2006a, 2006b; Johnson et al., 2004). Some studies have attempted to determine the indirect and semi-direct effects due to aerosols, whereas some have ignored the cloud lifetime effect. In this study, during the dust event accompanying with convective cloud development, a phenomenon related to the cloud lifetime effect is found.

On 16 July 2016, there were small amounts of aerosols with aerosol optical depths (AODs) less than 0.4 over the northern slope of the TP (Fig. 4a1), and large ice water path (IWP) values were distributed northwest of the TP (Fig. 4b1). Correspondingly, the cloud top height was high (Fig. 4d1) and the ice cloud particle radius was not large over the same area (Fig. 4c1). On 17 July 2016, a small number of aerosols remained to suspend over the northern region of the TP (Fig. 4a2). Compared with cloud features on 16 July, with the movement of clouds and the effects of aerosols, the IWP increases significantly, and the large IWP moves to northeast of the TP (Fig. 4b2). The cloud top height is still high, and the ice cloud particle radius over the same area decreases (Fig. 4c2 and Fig. 4d2). Due to the impact of aerosols, the ice cloud particle radius decreases; correspondingly, the cloud top height indicates higher convection, which implies that convective clouds develop because the cloud life is prolonged.

Fig. 5 shows the time series of the AOD and cloud properties from 16 to 17 July 2016 (yellow shaded area in Fig. 4). The AOD peaked over the northern TP, with a value of 0.16 from 16:00 UTC on 16 July to 01:00 UTC on 17 July, and then gradually declined. Corresponding to the change in aerosols, the ice particle radius over the northern TP reached a minimum on 17 July 2016; the cloud area fraction, cloud top height and relative humidity over the northern TP all increased initially and then decreased gradually after reaching their peak values. These variations in clouds are in agreement with the results of Myhre et al. (2007). As suggested in Myhre et al. (2007), the cloud cover is doubled when the AOD varies from 0.05 to 0.2, which is a result of aerosol-cloud interactions and a prolonged cloud lifetime. Sensitivity experiments in model simulation show that, given the water uptake of aerosols is considered, the cloud cover increases mostly with the AOD. Besides, Myhre et al. (2007) show an obvious dependence of cloud cover on the small AODs, which is in line with the suppression of the precipitation effect (aerosols mostly increase the cloud cover) and less with the semi-direct effect (aerosols mostly decrease the cloud cover). Because of the prolonged cloud lifetime, convective clouds could be developed. When the AOD increases to its peak value, the cloud top height is highest, and the cloud area fraction is the largest (Fig. 5). Simultaneously, dust is absorbing aerosol, the enhanced moisture convergence induced by the heating effect of dusts may be in favor of relative humidity (Lohmann and Feichter, 2001; Perlwitz and Miller, 2010; Huang et al., 2014). The variations in cloud properties imply that the effect of dust aerosols on convective clouds over the TP has promoted the development of convective clouds.

3.3. The eastward movement of dust-polluted convective clouds over the TP

Based on meteorological conditions, the movement of convective clouds can be preliminarily described. As shown in Fig. 6a and b, convective clouds originating from north of the TP moved northeastward on 16 July and 17 July 2016. As shown in Fig. 6c and d, after moving away from the TP, convective clouds continuously moved northeastward towards North China and southeastward towards South China. Furthermore, the movement of convective clouds from the TP was investigated by the distribution of TBB. According to the results of Maddox (1980), the low-value area of TBB corresponded to the area of increased convective activity, and the region where TBB was less than −10°C indicated an active area of convective clouds. The intensity of convective clouds was divided into 4 levels according to the TBB value: general convective clouds (−32 to −54°C), strong convective clouds accompanied by thunderstorms (−54 to −64°C), strong convective clouds passing through the troposphere (−64 to −80°C) and extremely convective clouds (less than −80°C). Fig. 7 shows the distribution of daily mean TBB; convective clouds were generated on 16 July over the northern TP and then moved southeast and northeast, which is consistent with the conclusion from meteorological conditions. On 18 July, the convective clouds reached North China and the Yangtze River basin and then developed and merged with local convective cloud clusters the next day.

As shown in Fig. 8a and b, strong convective clouds are mainly concentrated over 30°N-35°N and 80°E−90°E (i.e., the northern TP) on 16 July. Meanwhile, there is an abundance of convective clouds over 30°N-35°N and 110°E−120°E (i.e., South China) on 16 July. Thereafter, the convective clouds begin to move northward and southward the latitude and are concentrated over 27°N-40°N on 18 July and 31°N-40°N on 19 July (Fig. 8a). Simultaneously, the convective clouds move eastward with longitude and are concentrated over 95°E−110°E on 18 July and 110°E−120°E on 19 July (Fig. 8b). The convective clouds originating from South China gradually move eastward and extend

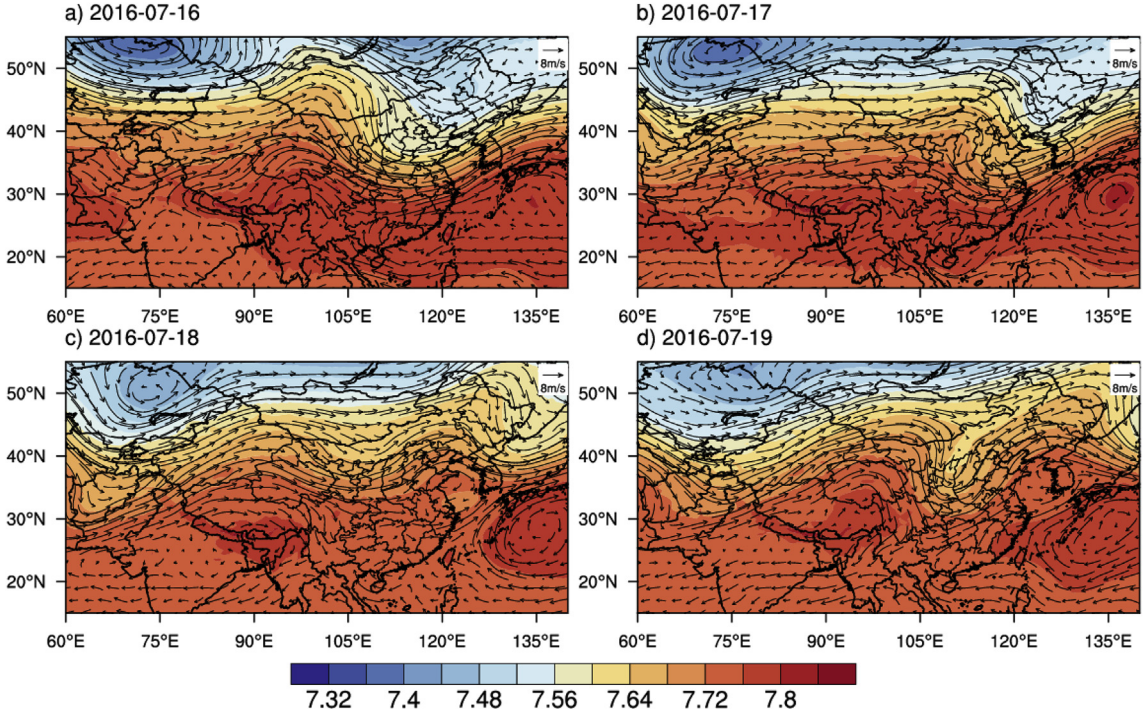

Fig. 6. Spatial distributions of the daily mean wind (vector; arrows) and geopotential height (colored; blue for low and red for high) at 400 hPa from MERRA-2 on 16–19 July 2016. (For interpretation of the references to color in this figure legend, the reader is referred to the Web version of this article.)

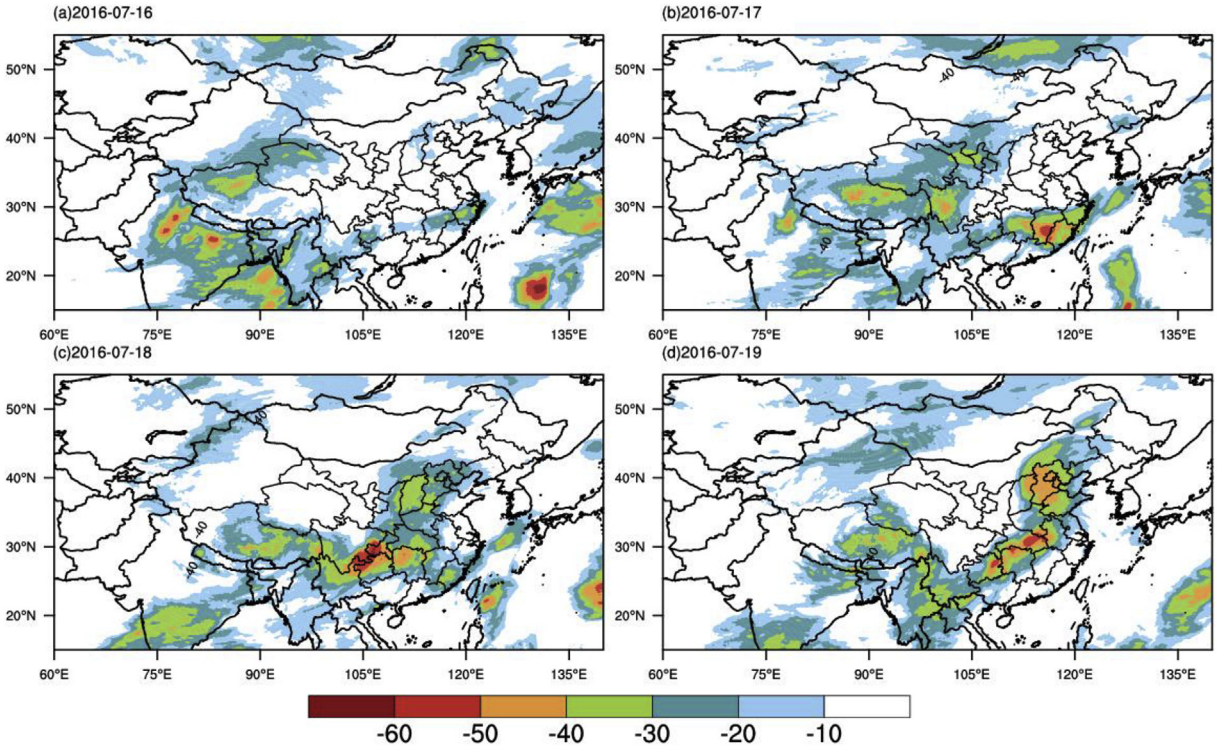

Fig. 7. Spatial distributions of the daily mean TBB (units: °C) from the FY-2E observations from 16 to 19 July 2016.

beyond 130°E on 18 July (Fig. 8b).

As illustrated above, here, the convective cloud is defined with TBB below −32 °C. The contour lines with TBB equaling −32 °C are plotted based on the hourly TBB data. The areas enclosed by the contour lines denote the TBB is below −32 °C, which are considered the positions of convective clouds occurring. Though it is limited by the time resolution of hourly TBB data, the convective position moving can be found based on hourly TBB data. Here, due to the limited space, we just show the convective positions at 00:15 UTC (blue lines in Fig. 9), 08:15 UTC (purple lines in Fig. 9) and 16:15 UTC (red lines in Fig. 9) of each day from 16 to 19 July 2016. Fig. 9a shows that there are many convective clouds over the northern TP, and there are also local convective clouds over South and North China. Based on the movements of convective clouds on 16 July 2016, convective clouds mainly originate over the

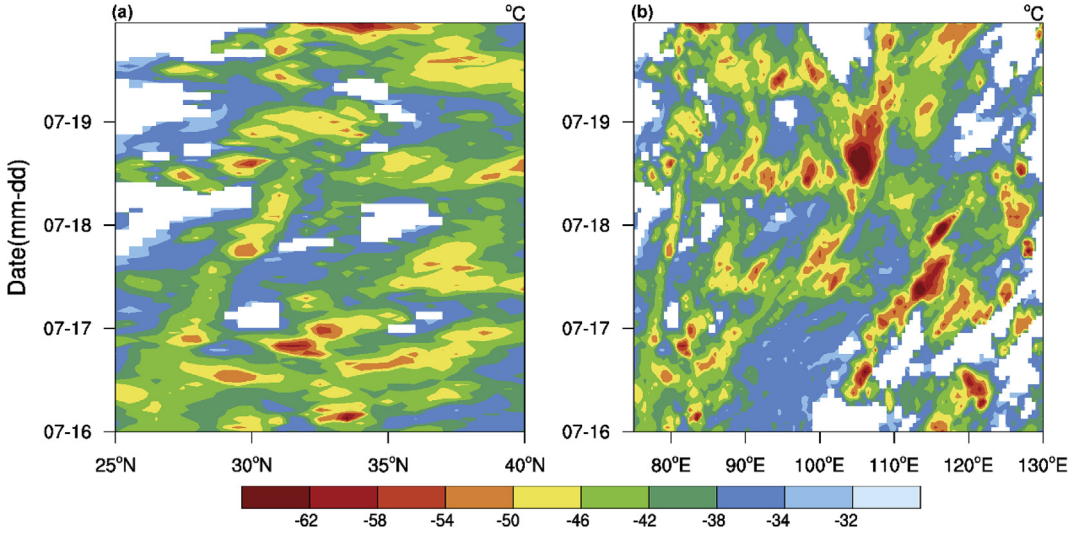

Fig. 8. Latitude-time cross-section of hourly TBBs less than −32°C averaged over the 75–130°E belt (a) and longitude-time section of hourly TBBs less than −32°C averaged over the 25–40°N belt (b) from 16–19 July 2016.

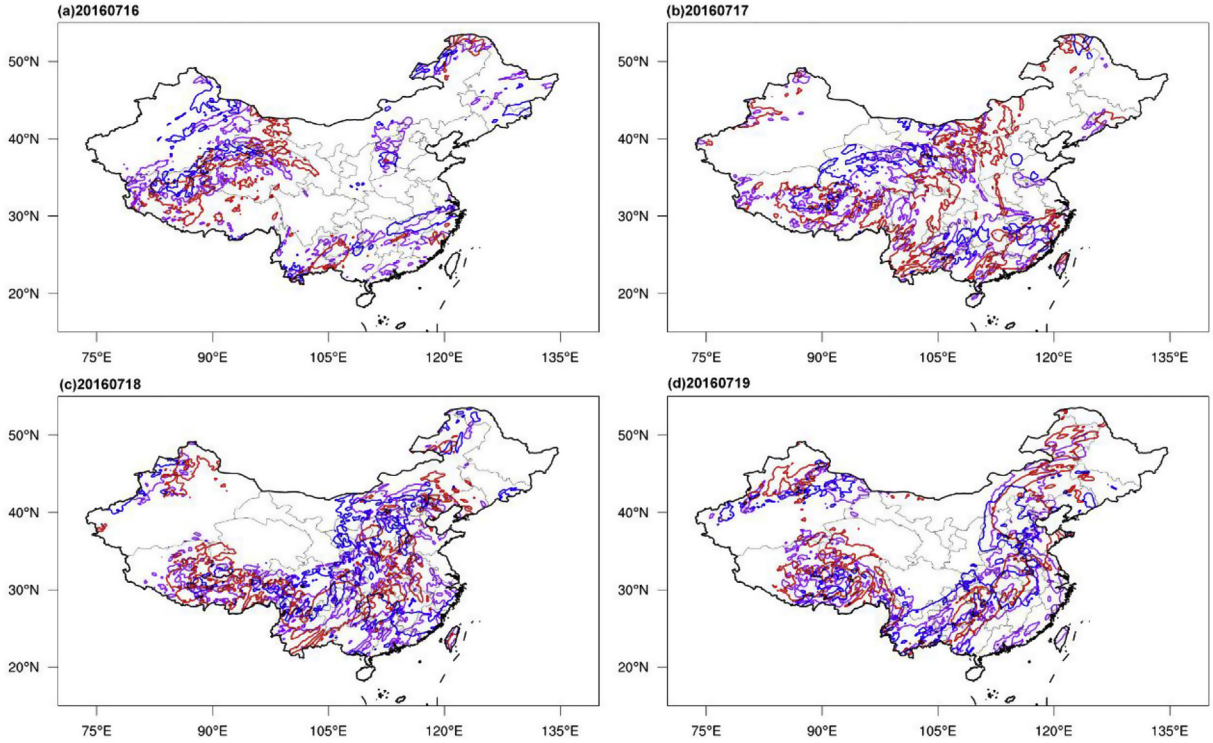

Fig. 9. Eastward movement of the convective cloud clusters from 16 to 19 July 2016. The contour lines represent a TBB equal to −32°C. The blue, purple and red lines correspond to convective cloud positions at 00:15 UTC, 08:15 UTC and 16:15 UTC, respectively. (For interpretation of the references to color in this figure legend, the reader is referred to the Web version of this article.)

northern TP and continue to move eastward. Thereafter, a portion of convective clouds originating over the northern part of the TP moved towards Northwest China and mixed with local convective clouds; the other portion of convective clouds moved over the Sichuan basin at 16:15 UTC on 17 July 2016 (Fig. 9b). Then, the convective clouds moved towards North China and the Yangtze River basin and merged with local convective clouds on 18 July 2016 (Fig. 9c). On 19 July, dispersed convective clouds developed and merged into large-area convective cloud clusters (Fig. 9d).

3.4. Impact of dust-polluted convective clouds from the TP on downstream precipitation

Fig. 10 shows time series of the 3-h cumulative precipitation over the Yangtze River basin (blue rectangle in Fig. 1) and North China (red rectangle in Fig. 1). Combining Figs. 5 and 10, after the AOD peak occurred in the early morning on 17 July, convective clouds moved eastward, merged with local convective clouds and brought rainfall over the Yangtze River basin. Finally, with continuous northward movement and merging, these clouds brought obvious rainfall over North China on 19 July 2016.

As shown in Fig. 11, with the convective clouds gradually moving

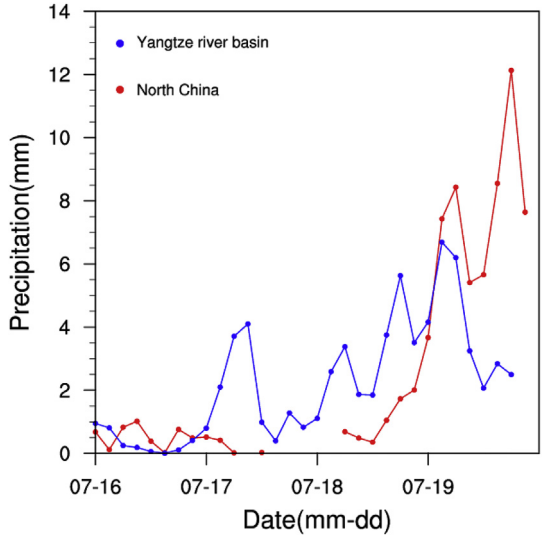

Fig. 10. Time series of 3-h cumulative precipitation over the Yangtze River basin (blue line) and North China (red line). (For interpretation of the references to color in this figure legend, the reader is referred to the Web version of this article.)

over the two regions, the daily cumulative precipitation over the Yangtze River basin and North China increased from 16 to 19 July 2016. On 19 July, convective clouds developed and merged into large-area convective cloud clusters. Meanwhile, along with the movement of convective cloud clusters, the aerosol-affected convective clouds continue to develop after outflowing from the TP. The ice water path (Fig. 12 c1 and d1) and cloud top height (Fig. 12 c2 and d2) increased continuously along the path of the cloud clusters, and the ice cloud particle radius reached a peak (Fig. 12 c3 and d3) on 19 July 2016 over these two regions and caused reginal heavy rainfall.

4. Conclusions

In this study, the indirect effect of aerosols on convective clouds over the TP and the impact of aerosol-affected convective clouds on precipitation over downstream areas are investigated. Based on the observations of the CALIPSO and CloudSat satellites, a mixture of dust aerosols and convective clouds over the TP is identified. By analyzing the evolution of AOD and cloud properties over the TP, we found that the addition of dust aerosols in clouds can induce a decrease in ice particle size and prolong the cloud lifetime. The cloud lifetime effect due to dust aerosols can enhance the development of convective clouds; correspondingly, the cloud top height and cloud area fraction increase. Driven by meteorological conditions, aerosol-affected convective clouds over the TP can move continuously towards the Yangtze River basin and North China within four days. Convective clouds over the TP move eastward and merge with local clusters, which triggers obvious and successive rainfall over the Yangtze River basin. Although the cloud lifetime effect due to dust aerosols occurs over the TP, the impact of dust-polluted convective clouds on downstream precipitation cannot be ignored.

Conflicts of interest

The authors declared that they have no conflicts of interest to this work.

We declare that we do not have any commercial or associative interest that represents a conflict of interest in connection with the work submitted.

Acknowledgements

This research was mainly supported by the Strategic Priority Research Program of Chinese Academy of Sciences (Grant No. XDA2006010301) and National Natural Science Foundation of China (91737101 and 91744311).

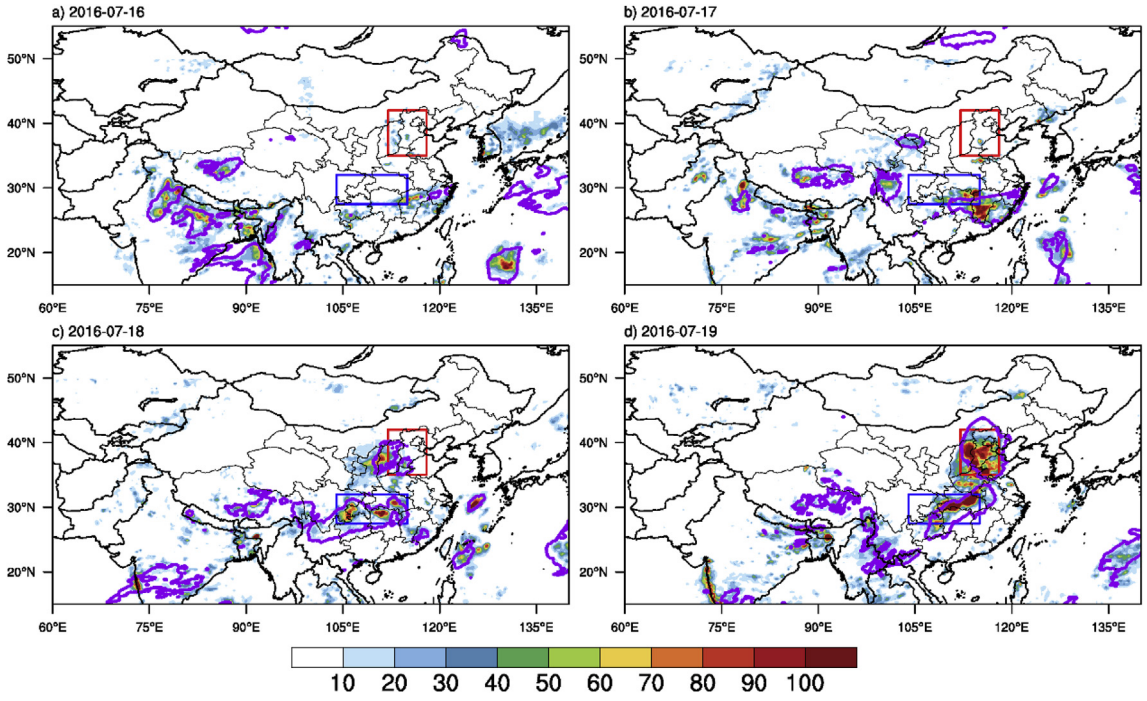

Fig. 11. Distributions of the daily cumulative precipitation (a–d) from 16 to 19 July 2016. The red and blue rectangles represent North China and the Yangtze River basin, respectively. The purple contour line denotes the convective cloud position where the daily mean TBB equals −32°C. (For interpretation of the references to color in this figure legend, the reader is referred to the Web version of this article.)

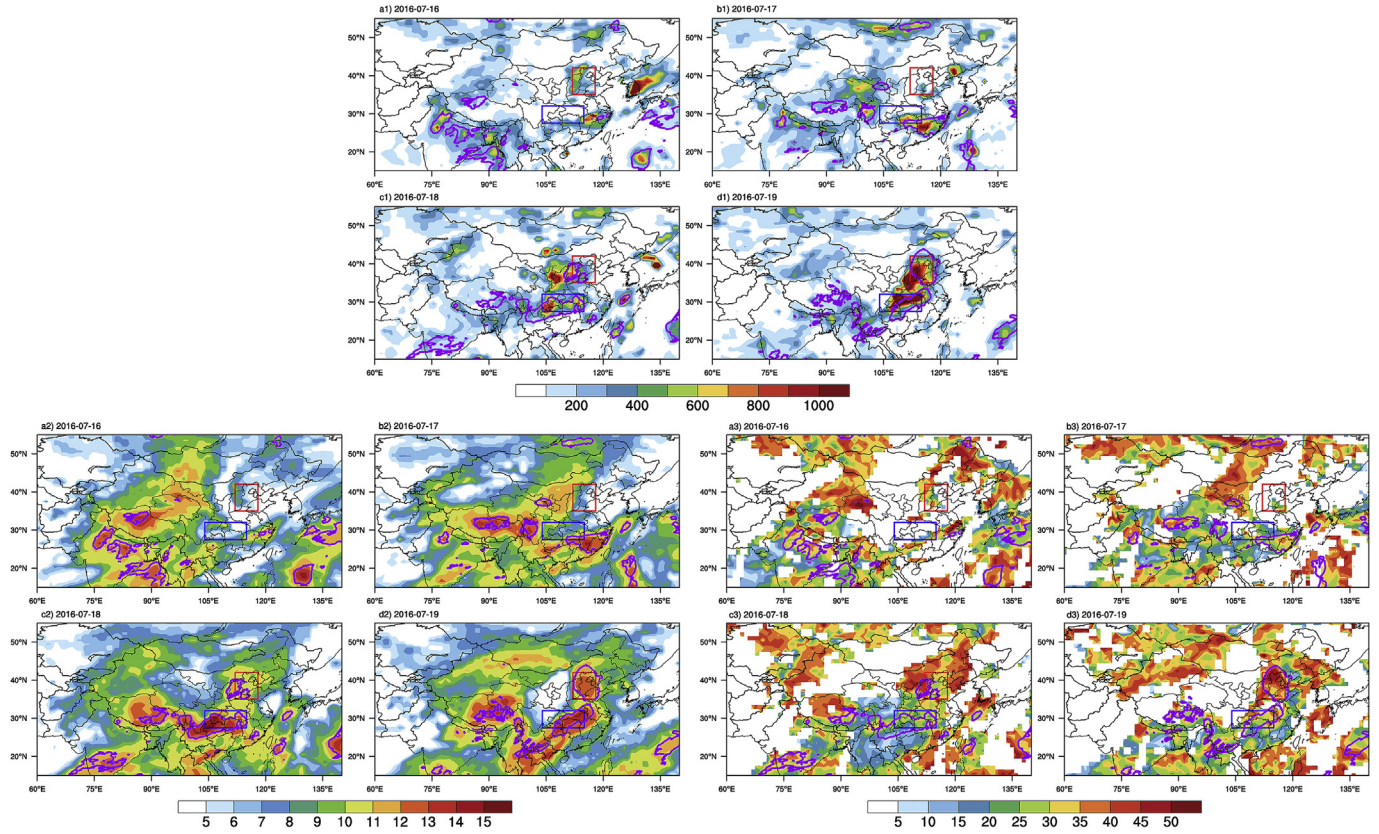

Fig. 12. Same as in Fig. 11 but for ice water path (a1-d1), cloud top height (a2-d2) and ice cloud particle radius (a3-d3).

Appendix A. Supplementary data

Supplementary data to this article can be found online at https://doi.org/10.1016/j.atmosenv.2019.04.001.

References

Ackerman, S.A., Strabala, K.I., Menzel, W.P., Frey, R.A., Moeller, C.C., Gumley, L.E., 1998. Discriminating clear sky from clouds with MODIS. J. Geophys. Res. 103 (D24), 32141. https://doi.org/10.1029/1998jd200032.

Andreae, M.Q., Rosenfeld, D., Artaxo, P., Costa, A.A., Frank, G.P., Longo, K.M., Silva-Dias, M., 2004. Smoking rain clouds over the Amazon. Science 303, 1337–1342. https://doi.org/10.1126/science.1092779.

Chambers, L.H., Lin, B., Young, D.F., 2002. Examination of new CERES data for evidence of tropical iris feedback. J. Clim. 15 (24), 3719–3726. https://doi.org/10.1175/1520-0442(2002)015<3719: EONCDF>2.0.CO;2.

Cook, J., Highwood, E.J., 2004. Climate response to tropospheric absorbing aerosols in an intermediate general-circulation model. Q. J. Roy. Meteorol. Soc. 130 (596), 175–191.

Duan, A., Wu, G., 2005. Role of the Tibetan Plateau thermal forcing in the summer climate patterns over subtropical Asia. Clim. Dyn. 24 (7–8), 793–807. https://doi.org/10.1007/s00382-004-0488-8.

Engel-Cox, J.A., Holloman, C.H., Coutant, B.W., Hoff, R.M., 2004. Qualitative and quantitative evaluation of MODIS satellite sensor data for regional and urban scale air quality. Atmos. Environ. 38 (16), 2495–2509.

Gelaro, R., Mccarty, W., Suárez, Max J., Todling, R., Molod, A., Takacs, L., Randles, C., Darmenov, A., Bosilovich, M.G., Reichle, R., Wargan, K., Coy, L., Cullather, R., Draper, C., Akella, S., Buchard, V., Conaty, A., da Silva, A., Gu, W., Kim, G.K., Koster, R., Lucchesi, R., Merkova, D., Nielsen, J.E., Partyka, G., Pawson, S., Putman, W., Rienecker, M., Schubert, S.D., Sienkiewicz, M., Zhao, B., 2017. The modern-era retrospective analysis for research and applications, version 2 (MERRA-2). J. Clim. 30 (14). https://doi.org/10.1175/JCLI-D-16-0758.1.

Hansen, J., Sato, M., Ruedy, R., 1997. Radiative forcing and climate response. J. Geophys. Res.: Atmos. 102 (D6), 6831–6864. https://doi.org/10.1029/96JD03436.

Hersbach, H., 2016. The ERA5 atmospheric reanalysis. In: AGU Fall Meeting. AGU Fall Meeting Abstracts.

Hua, S., Liu, Y., Jia, R., Chang, S.T., Wu, C.Q., Zhu, Q.Z., Shao, T.B., Wang, B., 2018. Role of clouds in accelerating cold-season warming during 2000–2015 over the Tibetan Plateau. Int. J. Climatol. 1–17. https://doi.org/10.1002/joc.5709.

Huang, J., Minnis, P., Lin, B., Wang, T., Yi, Y., Hu, Y., Sun-Mack, S., Ayers, J., 2006a. Possible influences of Asian dust aerosols on cloud properties and radiative forcing observed from MODIS and CERES. Geophys. Res. Lett. 33 (33), 272–288. https://doi.org/10.1029/2005gl024724.

Huang, J., Lin, B., Minnis, P., Wang, T., Wang, X., Hu, Y., Yi, Y., Ayers, J., 2006b. Satellite-based assessment of possible dust aerosols semi-direct effect on cloud water path over East Asia. Geophys. Res. Lett. 33, L19802. https://doi.org/10.1029/2006GL026561.

Huang, J., Fu, Q., Su, J., Tang, Q., Minnis, P., Hu, Y., Yi, Y., Zhao, Q., 2009. Taklimakan dust aerosol radiative heating derived from CALIPSO observations using the Fu-Liou radiation model with CERES constraints. Atmos. Chem. Phys. 9 (12), 4011–4021. https://doi.org/10.5194/acp-9-4011-2009.

Huang, J., Minnis, P., Yan, H., Yi, Y., Chen, B., Zhang, L., Ayers, J.K., 2010. Dust aerosol effect on semi-arid climate over Northwest China detected from A-Train satellite measurements. Atmos. Chem. Phys. 10, 6863–6872. https://doi.org/10.5194/acp-10-6863-2010.

Huang, J., Wang, T., Wang, W., Li, Z., Yan, H., 2014. Climate effects of dust aerosols over East Asian arid and semiarid regions. J. Geophys. Res. Atmos. 119, 11398–11416. https://doi.org/10.1002/2014JD021796.

Jia, R., Liu, Y., Chen, B., Zhang, Z., Huang, J., 2015. Source and transportation of summer dust over the Tibetan Plateau. Atmos. Environ. 123, 210–219. https://doi.org/10.1016/j.atmosenv.2015.10.038.

Johnson, B.T., Shine, K.P., Forster, P.M., 2004. The semi-direct aerosol effect: impact of absorbing aerosols on marine stratocumulus. Q. J. Roy. Meteorol. Soc. 130 (599), 1407–1422. https://doi.org/10.1256/qj.03.61.

Khain, A.P., BenMoshe, N., Pokrovsky, A., 2008. Factors determining the impact of aerosols on surface precipitation from clouds: an attempt at classification. J. Atmos. Sci. 65, 1721–1748. https://doi.org/10.1175/2007JAS2515.1.

Koch, D., Genio, A.D., 2010. Black carbon absorption effects on cloud cover, review and synthesis. Atmos. Chem. Phys. 10 (3), 7323–7346.

Kuhlmann, J., Quaas, J., 2010. How can aerosols affect the Asian summer monsoon? Assessment during three consecutive pre-monsoon seasons from CALIPSO satellite data. Atmos. Chem. Phys. 10 4673e4688.

Liu, Z.Y., Vaughan, M., Winker, D., Kittaka, C., Getzewich, B., Kuehn, R., Omar, A., Powell, K., Trepte, C., Hostetler, C., 2009. The CALIPSO Lidar cloud and aerosol discrimination: version 2 algorithm and initial assessment of performance. J. Atmos. Ocean. Technol. 26, 1198–1213. https://doi.org/10.1175/2009JTECHA1229.1.

Liu, X., Li, W.P., Xu, H.X., Wu, G.X., 2007. The effect of Tibetan plateau heating on the East asian summer precipitation. Plateau Meteorol. 26 (6), 1287–1292. https://doi.org/10.1002/jrs.1570.

Liu, Y., Shi, G., Xie, Y., 2013. Impact of smoke aerosol on glacial-interglacial climate. Adv. Atmos. Sci. 30 (6), 1725–1731. https://doi.org/10.1007/s00376-013-2289-7.

Liu, Y., Jia, R., Dai, T., Xie, Y., Shi, G., 2014. A review of aerosol optical properties and radiative effects. J. Meteor. Res. 28 (6), 1003–1028. https://doi.org/10.1007/s13351-014-4045-z.

Liu, Y., Sato, Y., Jia, R., Xie, Y., Huang, J., Nakajima, T., 2015. Modeling study on the transport of summer dust and anthropogenic aerosols over the Tibetan Plateau. Atmos. Chem. Phys. 15 (21), 12581–12594. https://doi.org/10.5194/acp-15-12581-2015.

Lau, W.K.M., Kim, M.K., Kim, K.M., Lee, W.S., 2010. Enhanced surface warming and accelerated snow melt in the Himalayas and Tibetan Plateau induced by absorbing aerosols. Environ. Res. Lett. 5 (2), 025204. https://doi.org/10.1088/1748-9326/5/2/025204.

Lohmann, U., Feichter, J., 2001. Can the direct and semi-direct aerosol effect compete with the indirect effect on a global scale? Geophys. Res. Lett. 28, 159–161. https://doi.org/10.1029/2000GL012051.

Lonfat, M., 2004. Precipitation distribution in tropical cyclones using the tropical rainfall measuring mission (TRMM) microwave imager: a global perspective. Health Res. Policy Syst. 11 (1). https://doi.org/10.1186/1478-4505-11-40. 40-40.

Manabe, S., Terpstra, T.B., 1974. The effects of mountains on the general circulation of the atmosphere as identified by numerical experiments. J. Atmos. Sci. 31 (1), 3–42.

Maddox, R.A., 1980. Mesoscale convective complexes. Bull. Am. Meteorol. Soc. 61 (11), 1374–1387.

Menon, S., Hansen, J., Nazarenko, L., Luo, Y.F., 2002. Climate effects of black carbon aerosols in China and India. Science 297 (5590), 2250–2253.

Molod, A., Takacs, L., Suarez, M., Bacmeister, J., 2015. Development of the GEOS-5 atmospheric general circulation model: evolution from MERRA to MERRA2. Geosci. Model Dev. (GMD) 8 (5), 1339–1356. https://doi.org/10.5194/gmd-8-1339-2015.

Myhre, G., Stordal, F., Johnsrud, M., Kaufman, Y.J., Rosenfeld, D., Storelvmo, T., Kristjansson, J.E., Berntsen, T.K., Myhre, A., Isaksen, I.S.A., 2007. Aerosol-cloud interaction inferred from MODIS satellite data and global aerosol models. Atmos. Chem. Phys. 7 (12), 3081–3101. https://doi.org/10.5194/acp-7-3081-2007.

Petters, M.D., Snider, J.R., Stevens, B., Vali, G., Faloona, I., Russell, L.M., 2006. Accumulation mode aerosol, pockets of open cells, and particle nucleation in the remote subtropical Pacific marine boundary layer. J. Geophys. Res. 111https://doi.org/10.1029/2004JD005694. D02206.

Perlwitz, J., Miller, R.L., 2010. Cloud cover increase with increasing aerosol absorptivity-A counterexample to the conventional semi-direct aerosol effect. J. Geophys. Res. 115https://doi.org/10.1029/2009JD012637. D08203.

Qin, S.G., Tang, J., Wen, Y.P., 2001. Black carbon and its importance in climate change studies. Meteorol. Mon. 27 (11), 3–7.

Qian, Y., Gong, D., Fan, J., Leung, L.R., Bennartz, R., Chen, D.L., Wang, W.G., 2009. Heavy pollution suppresses light rain in China: observations and modeling. J. Geophys. Res. Atmos. 114 (15), 0–2. https://doi.org/10.1029/2008JD011575.

Rosenfeld, D., Woodley, W.L., 2000. Deep convective clouds with sustained supercooled liquid water down to –37.5°C. Nature 405, 440–442. https://doi.org/10.1038/35013030.

Rosenfeld, D., Lohmann, U., Raga, G.B., O'Dowd, C.D., Kulmala, M., Fuzzi, S., Reissell, A., Andreae, M.O., 2008. Flood or drought: how do aerosol affect precipitation? Science 321, 1309–1313.

Rosenfeld, D., Sherwood, S., Wood, R., Donner, L., 2014. Climate effects of aerosol-cloud interactions. Science 343 (6169), 379–380. https://doi.org/10.1126/science.1247490.

Sassen, W.K., 2002. Cirrus cloud microphysical property retrieval using lidar and radar measurements. part ii: midlatitude cirrus microphysical and radiative properties. J. Atmos. Sci. 59 (14), 2291–2302. https://doi.org/10.1175/1520-0469(2002)059<2291: CCMPRU>2.0.CO;2.

Sokolik, I.N., Toon, O.B., 1996. Direct radiative forcing by anthropogenic airborne mineral aerosols. Nature 381, 681–683. https://doi.org/10.1038/381681a0.

Shi, G., Wang, H., Wang, B., Li, W., Gong, S., Zhao, T., 2005. Sensitivity experiments on the effects of optical properties of dust aerosols on their radiative forcing under clear sky condition. J. Meteorol. Soc. Jpn. 83A, 333–346.

Shi, Z., Liu, X., Liu, Y., Sha, Y., Xu, T., 2015. Impact of Mongolian plateau versus Tibetan plateau on the westerly jet over north pacific ocean. Clim. Dyn. 44 (11), 3067–3076. https://doi.org/10.1007/s00382-014-2217-2.

Simpson, J., Adler, R.F., North, G.R., 1988. A proposed tropical rainfall measuring mission (TRMM). Meteorol. Atmos. Phys. 60 (1–3), 19–36. https://doi.org/10.1007/BF01029783.

Stephens, G.L., Vane, D.G., Tanelli, S., Im, E., Durden, S., Rokey, M., Reinke, D., Partain, P., Mace, G.G., Austin, R., L'Ecuyer, T., Haynes, J., Lebsock, M., Suzuki, K., Waliser, D., Wu, D., Kay, J., Gettelman, A., Wang, Z., Marchand, R., 2008. Cloudsat mission: performance and early science after the first year of operation. J. Geophys. Res-Atmos. 113 (D8), 2036–2044. https://doi.org/10.1029/2008JD009982.

Tao, W.K., Chen, J.P., Li, Z., Wang, C., Zhang, C., 2012. Impact of aerosols on convective clouds and precipitation. Rev. Geophys. 50https://doi.org/10.1029/2011RG000369. RG2001.

Tang, H., Micheels, A., Eronen, J.T., Ahrens, B., Fortelius, M., 2013. Asynchronous responses of East Asian and Indian summer monsoons to mountain uplift shown by regional climate modelling experiments. Clim. Dyn. 40 (5–6), 1531–1549. https://doi.org/10.1007/s00382-012-1603-x.

Vane, D., Stephens, G.L., 2008. The CloudSat mission and the A-train: a revolutionary approach to observing Earth's atmosphere. In: Aerospace Conference. IEEE.

Wang, W., Huang, J., Minnis, P., Hu, Y., Li, J., Huang, Z., et al., 2010. Dusty cloud properties and radiative forcing over dust source and downwind regions derived from A-train data during the pacific dust experiment. J. Geophys. Res. Atmos. 115 (D4). https://doi.org/10.1029/2010JD014109.

Wang, X., Li, X., 2014. Preliminary investigation of FengYun-3C microwave temperature sounder (MWTS) measurements. Remote Sens. Lett. 5 (12), 10. https://doi.org/10.1080/2150704X.2014.988305.

Wang, X., Pu, W., Zhang, X., Ren, Y., Huang, J., 2015. Water-soluble ions and trace elements in surface snow and their potential source regions across northeastern China. Atmos. Environ. 114, 57–65. https://doi.org/10.1016/j.atmosenv.2015.05.012.

Winker, D.M., Pelon, J., 2004. The CALIPSO mission. In: IEEE International Geoscience & Remote Sensing Symposium. IEEE.

Wu, G., Liu, Y., Zhang, Q., Duan, A., Wang, T., Wan, R., Liu, X., Li, W., Wang, Z., Liang, X., 2007. The influence of mechanical and thermal forcing by the Tibetan Plateau on Asian climate. J. Hydrometeorol. 8 (4), 770–789. https://doi.org/10.1175/JHM609.1.

Zhang, X.Y., Arimoto, R., Cao, J.J., An, Z.S., Wang, D., 2001. Atmospheric dust aerosol over the Tibetan Plateau. J. Geophys. Res. Atmos. 106, 18471–18476. https://doi.org/10.1029/2000JD900672.

Zhang, R.Y., 2010. Getting to the critical nucleus of aerosol formation. Science 328 (5984), 1366–1367. https://doi.org/10.1126/science.1189732.

Zhou, X., Zhao, P., Chen, J., Chen, L.X., Li, W.L., 2009. Impacts of thermodynamic processes over the Tibetan plateau on the northern hemispheric climate. Sci. China D Earth Sci. 52 (11), 1679–1693. https://doi.org/10.1007/s11430-009-0194-9.

Zou, X., Wang, X., Weng, F., Li, G., 2011. Assessments of Chinese Fengyun microwave temperature sounder (MWTS) measurements for weather and climate applications. J. Atmos. Ocean. Technol. 28, 1206–1227. https://doi.org/10.1175/JTECH-D-11-00023.1.